DOT/FAA/AR-99/86

Office of Aviation Research
Washington, D.C. 20591

The Effects of Angular Orientation on Flame Spread Over Thin Materials

December 1999

Final Report

This document is available to the U.S. public through the National Technical Information Service (NTIS), Springfield, Virginia 22161.

U.S. Department of Transportation
Federal Aviation Administration

NOTICE

This document is disseminated under the sponsorship of the U.S. Department of Transportation in the interest of information exchange. The United States Government assumes no liability for the contents or use thereof. The United States Government does not endorse products or manufacturers. Trade or manufacturer's names appear herein solely because they are considered essential to the objective of this report. This document does not constitute FAA certification policy. Consult your local FAA aircraft certification office as to its use.

This report is available at the Federal Aviation Administration William J. Hughes Technical Center's Full-Text Technical Reports page: www.actlibrary.act.faa.gov in Adobe Acrobat portable document form (PDF).

Technical Report Documentation Page

1. Report No.	2. Government Accession No.	3. Recipient's Catalog No.
DOT/FAA/AR-99/86		

4. Title and Subtitle	5. Report Date
THE EFFECTS OF ANGULAR ORIENTATION ON FLAME SPREAD OVER THIN MATERIALS	December 1999
	6. Performing Organization Code

7. Author(s)	8. Performing Organization Report No.
J. G. Quintiere	

9. Performing Organization Name and Address	10. Work Unit No. (TRAIS)
University of Maryland Department of Fire Protection Engineering College Park, MD 20742	11. Contract or Grant No.

12. Sponsoring Agency Name and Address	13. Type of Report and Period Covered
U.S. Department of Transportation Federal Aviation Administration Office of Aviation Research Washington, DC 20591	Final Report
	14. Sponsoring Agency Code ANM-100

15. Supplementary Notes

The Federal Aviation Administration William J. Hughes Technical Center technical manager was Gus Sarkos.

16. Abstract

Data were taken to show the flame spread characteristics of thin materials burning on an insulating substrate. Metalized polyethylene terephthalate (0.20 mm) and paper (0.17 mm) were burned on the surface of glass fiber insulation. Flame spread was measured in the upward or downward facing orientation for the material and in the directions of gravity assistance (up) or gravity opposition (down). Measurements were taken at various angles ranging from a vertical to a horizontal orientation.

A theoretical analysis was developed to predict the flame spread as a function of material properties, sample orientation, and flame spread direction. The one-dimensional theory was in reasonable agreement with paper data. Vertical upward spread was found to yield the highest velocity.

17. Key Words	18. Distribution Statement
Flame spread, Thin films, Polymer, Flammability, Fire, Fire hazard	This document is available to the public through the National Technical Information Service (NTIS), Springfield, Virginia 22161.

19. Security Classif. (of this report)	20. Security Classif. (of this page)	21. No. of Pages	22. Price
Unclassified	Unclassified	34	

ACKNOWLEDGEMENTS

The author is indebted to Sanjeev Gandhi and Sean Crowley for their help in designing the test apparatus and conducting the experiments, to Richard Lyon for his helpful discussions, and to Patricia Cahill for useful discussions and guidance on the flammability and characteristics of thin film acoustic insulation.

TABLE OF CONTENTS

LIST OF FIGURES

LIST OF TABLES

EXECUTIVE SUMMARY

Data were taken to show the flame spread characteristics of thin materials burning on an insulating substrate. Metalized polyethylene terephthalate (0.20 mm) and paper (0.17 mm) were burned on the surface of glass fiber insulation. Flame spread was measured in the upward or downward facing orientation for the material and in the directions of gravity assistance (up) or gravity opposition (down). Measurements were taken at various angles ranging from a vertical to a horizontal orientation.

A theoretical analysis was developed to predict the flame spread as a function of material properties, sample orientation, and flame spread direction. The one-dimensional theory was in reasonable agreement with the paper data. Vertical upward spread was found to yield the highest velocity.

INTRODUCTION

This study was motivated by the need to investigate the flammability of aircraft thermal-acoustical insulation blankets. In particular, it considers the thin-film material which encapsulates the insulation material. As formed into blankets, the insulation lines the interior skin of aircraft cabins to reduce the noise and heat transfer.

Two small-scale flame spread tests apply to thermal-acoustical insulation blankets. The first is a regulatory requirement contained in FAR 25.853, a vertical Bunsen burner test. The second is an industry standard called the "cotton swab test," which consists of ignition by alcohol-soaked cotton swabs inserted in the center of a horizontal sample and at the crease it makes with a vertical section [1].

Attempts to simulate realistic ignition sources were conducted by Cahill [2]. One example, of upward and downward spread on a metalized polyethylene terephthalate (PET) film insulation blanket is shown in figure 1 on a curved aircraft cabin section. The maximum upward burnout region (U_b), downward pyrolysis region (D_p), and upward flame length (L_f) were measured from a video recording of the test. Despite erratic burn fronts with discontinuous flaming regions, the maximum speeds and flame lengths appear approximately constant at speeds of 5.9 mm/s up, 2.6 mm/s down, and lengths of 120 mm for the upward flames.

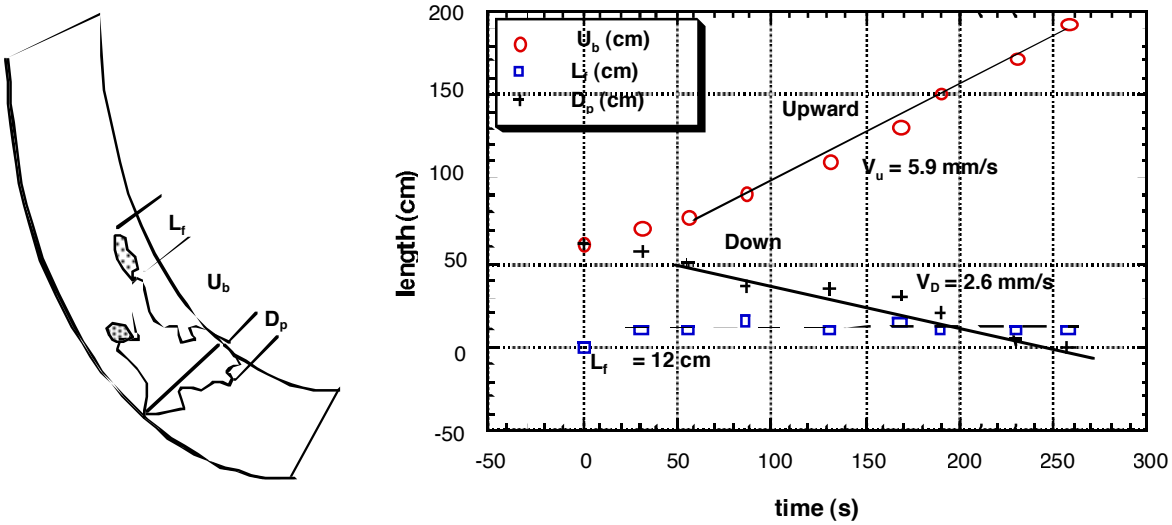

FIGURE 1. FLAME SPREAD ON A METALIZED PET-FIBERGLASS INSULATION FILM AFTER IGNITION BY AN ELECTRICAL ARC

It was generally found that the ignition and sustained flame spread of typical aircraft insulation blanket films were difficult to achieve by small flame sources. Some speculated that Bunsen burner type testing for samples oriented downward and 45° with the vertical gave more consistent spread. As a consequence, it was decided to investigate the effect of orientation and inclination angle on the flame spread of thin films. A metalized PET film, which seemed easily ignitable by a small flame, was selected as a representative aircraft material. Later it was found that a thin-paper specimen gave more consistent one-dimensional flame spread results. Both upward and downward flame spread was examined.

EXPERIMENTAL ARRANGEMENT

The experimental test apparatus consisted of a steel holder that could sandwich a test sample film against fiberglass insulation without compression. The apparatus is shown in figure 2. A grid was inscribed at 0.5-inch (1.27-cm) increments on each outward facing steel longitudinal edge. This enabled an observer to identify the flame position. A digital clock was positioned so that the time and flame position could be simultaneously viewed on a video recording. For burning on the underside of the sample, a mirror was positioned to observe the clock and the flame progression. A rod attached to one face of the steel holder and a clamp arrangement allowed the assembly to be rotated. A level gage and protractor was used to set the angle, ϕ, to the vertical.

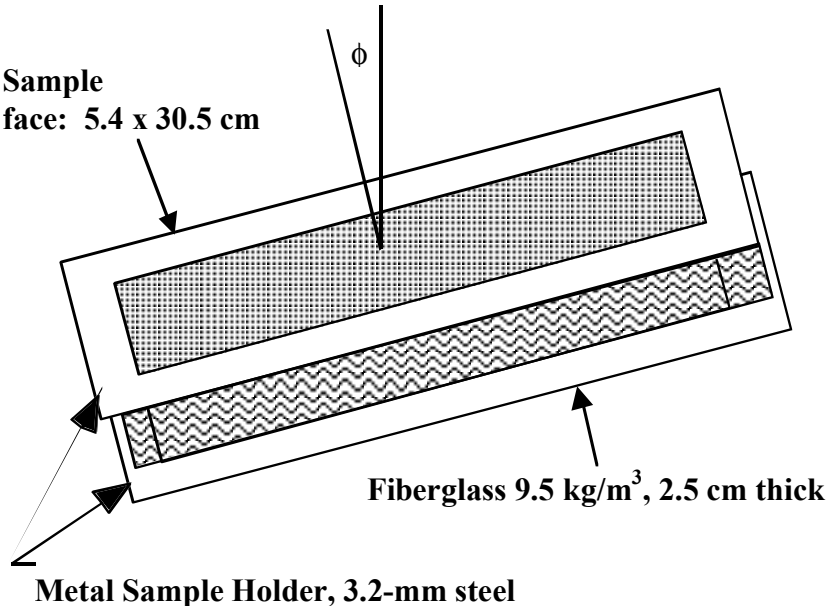

FIGURE 2. FLAME SPREAD APPARATUS

A small butane diffusion flame approximately 1-2 cm in length and 1 cm in diameter was used to ignite the film sample. Once ignition occurred, the igniter was withdrawn. If flame spread terminated before the end of the 12-inch (30.5-cm) sample length, the igniter was reapplied. This was repeated as necessary.

Two samples were tested. The first was representative of aircraft thermal-acoustical films; the second was a brown paper towel (napkin) commonly found in dispensers for drying hands. The latter was selected because the metalized polyethylene terephthalate (PET) did not always sustain flame spread, and a more consistent material was desired. It was found that the paper napkin did yield similar results to the PET, and it also had similar properties. Component material properties are shown in table 1.

TABLE 1. PHYSICAL PROPERTIES

Material	Thickness (δ) (mm)	Density (ρ) (g/cm^3)	Surface Density (ρδ) (g/m^2)
Met. PET	0.201	0.18	35.6
Paper Napkin	0.168	0.22	37.4
Fiberglass	25.4	0.0095 or $(0.59 b \frac{Lb}{ft^3})$	242.5

The samples were tested over angles ranging from 90° (vertical) to 0° (horizontal). A designation of "+ϕ" represents an upward facing sample (top) and "-ϕ" a downward facing sample (bottom). Both upward and downward spread was examined. Figures 3a-3g show the progression of the flame tip position as a function of time for the paper napkin. The position was always estimated by the tip of the visible flame in the direction of spread. The rate of movement of the flame tip will represent the speed of the pyrolysis front provided the speed is constant. For accelerating upward spread, the pyrolysis front speed would be less than flame tip speed. All measurements were made under laboratory conditions of approximately 23 ± 2°C and 50 ± 5% relative humidity.

THEORETICAL MODEL

Several studies are significant in constructing the theoretical model used. The important processes in flame spread can be separated into two parts: (1) the rate of heat transfer to material ahead of the pyrolysis front and (2) the time of ignition for this newly heated material. The following concepts originate from a study on upward flame spread over textiles at angles of 0° to 60° with the vertical [3]. Figure 4 shows the typical flame spread configuration. The pyrolysis length is denoted by x_p and the flame length is denoted by x_f as measured from the rear of the pyrolysis region. In figure 4, the flame spread is shown, for convenience, to be simultaneously spreading up and down. In reality, there would be a burnout region following the "rear" of the pyrolysis region in each case, which is not shown in figure 4.

For a thermally thin material heated from one side by a flame plume, flame speed, υ_p or rate of change of x_p is given as

$$\upsilon_p = \frac{\int_{x_p}^{\infty} \dot{q}'' dx}{\rho \delta c (T_{ig} - T_\infty)} \tag{1}$$

where ρ is density
δ is thickness
c is specific heat
T_{ig} is ignition temperature
T_∞ is initial or ambient temperature
$\dot{q}''$ is the net surface heat flux to the material

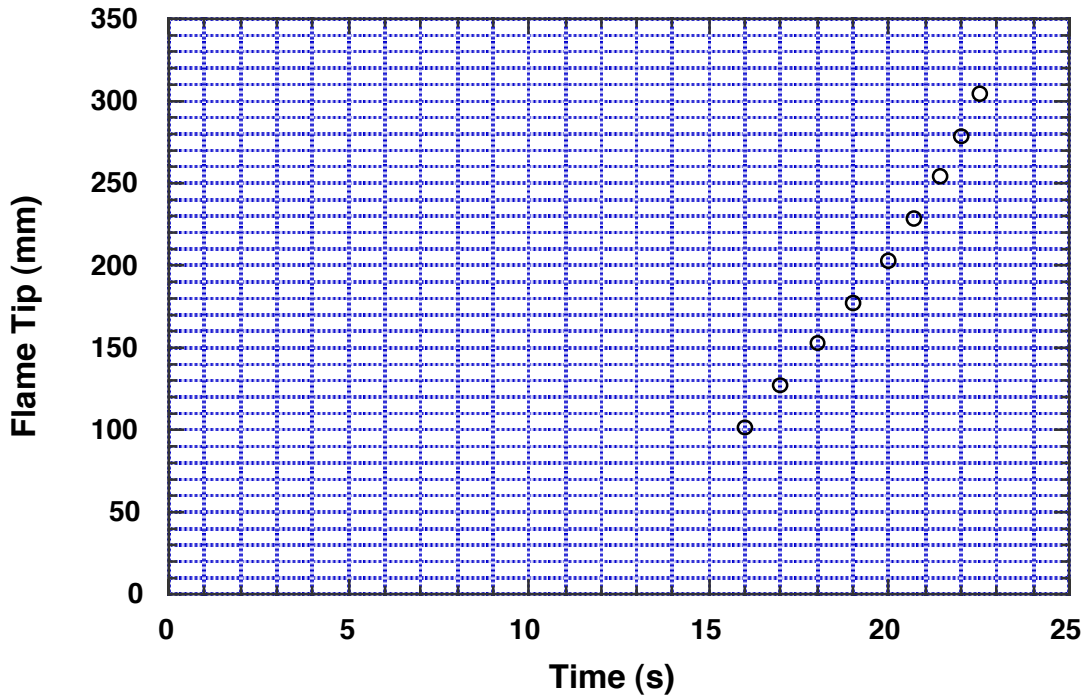

FIGURE 3a. UPWARD FLAME SPREAD, $\phi = 0°$, NAPKIN

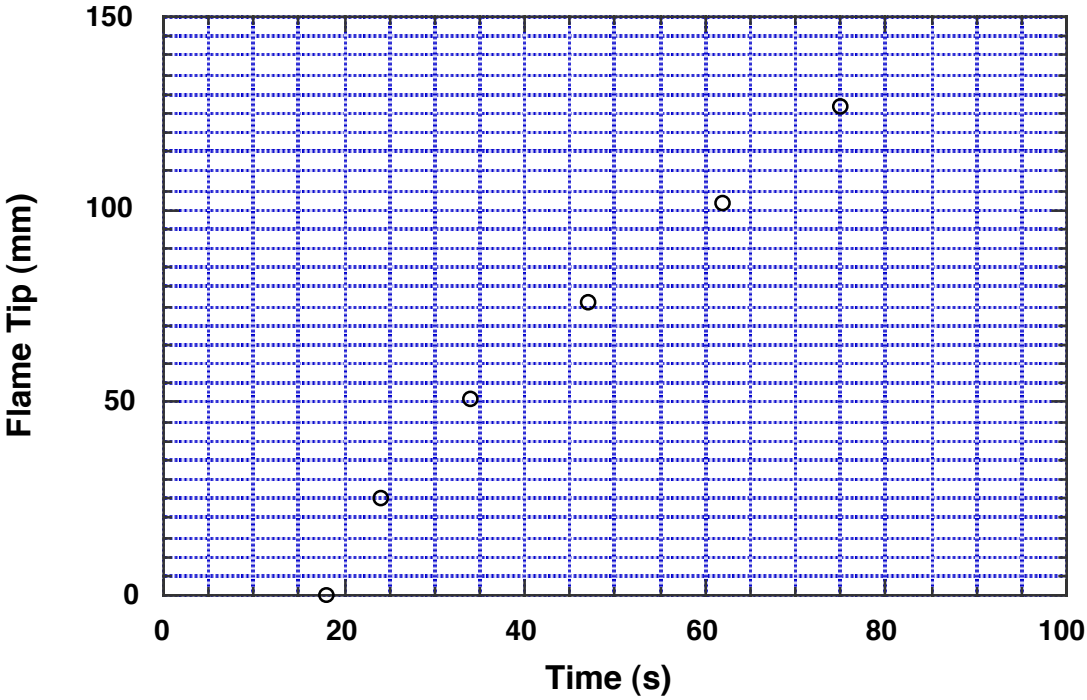

FIGURE 3b. DOWNWARD FLAME SPREAD, $\phi = 0°$, NAPKIN

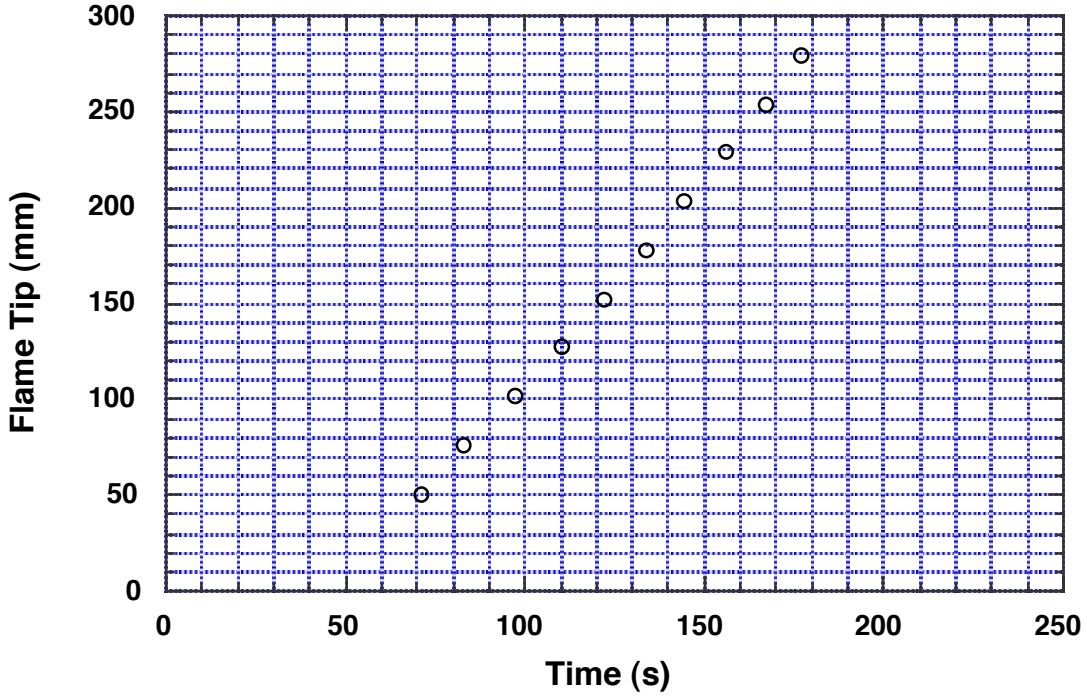

FIGURE 3c. HORIZONTAL FLAME SPREAD, FACING UP, ϕ = +90°, NAPKIN

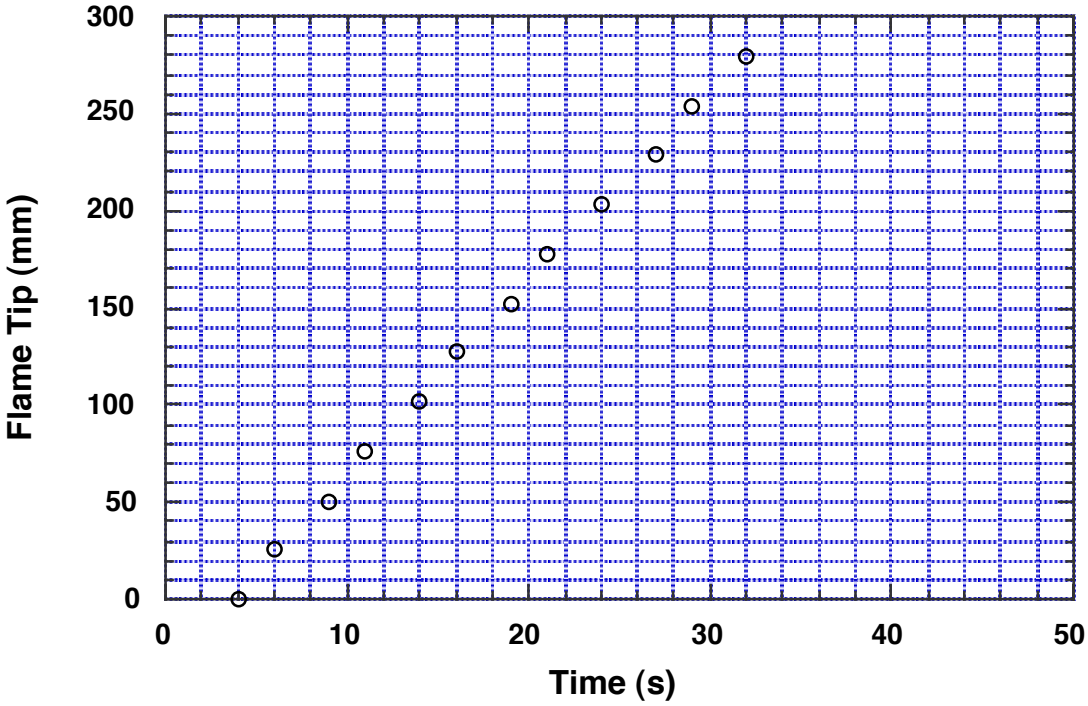

FIGURE 3d. HORIZONTAL FLAME SPREAD, FACING DOWN, ϕ = -90°, NAPKIN

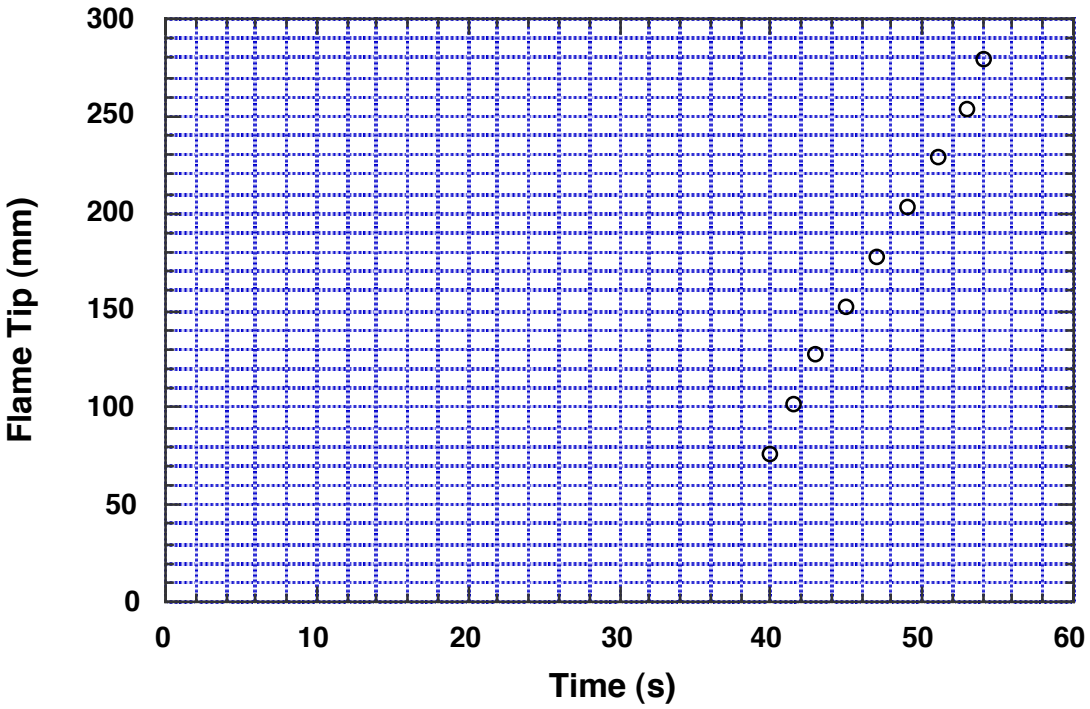

FIGURE 3e. UPWARD FLAME SPREAD, FACING UP, ϕ = +30°, NAPKIN

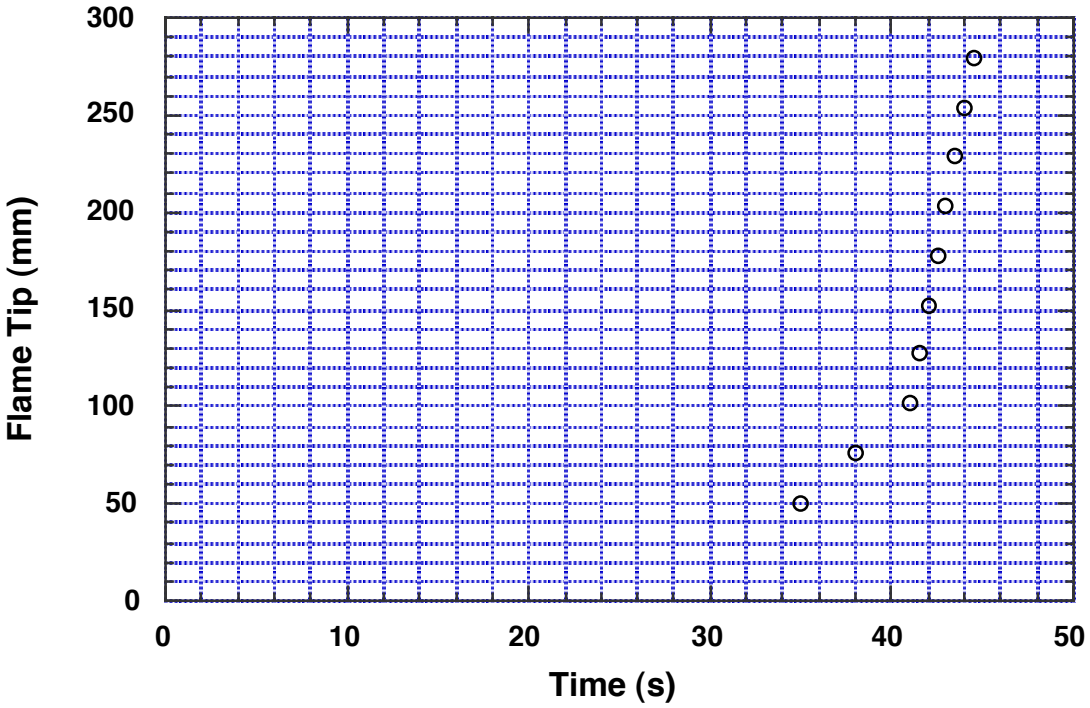

FIGURE 3f. UPWARD FLAME SPREAD, FACING DOWN, ϕ = -30°, NAPKIN

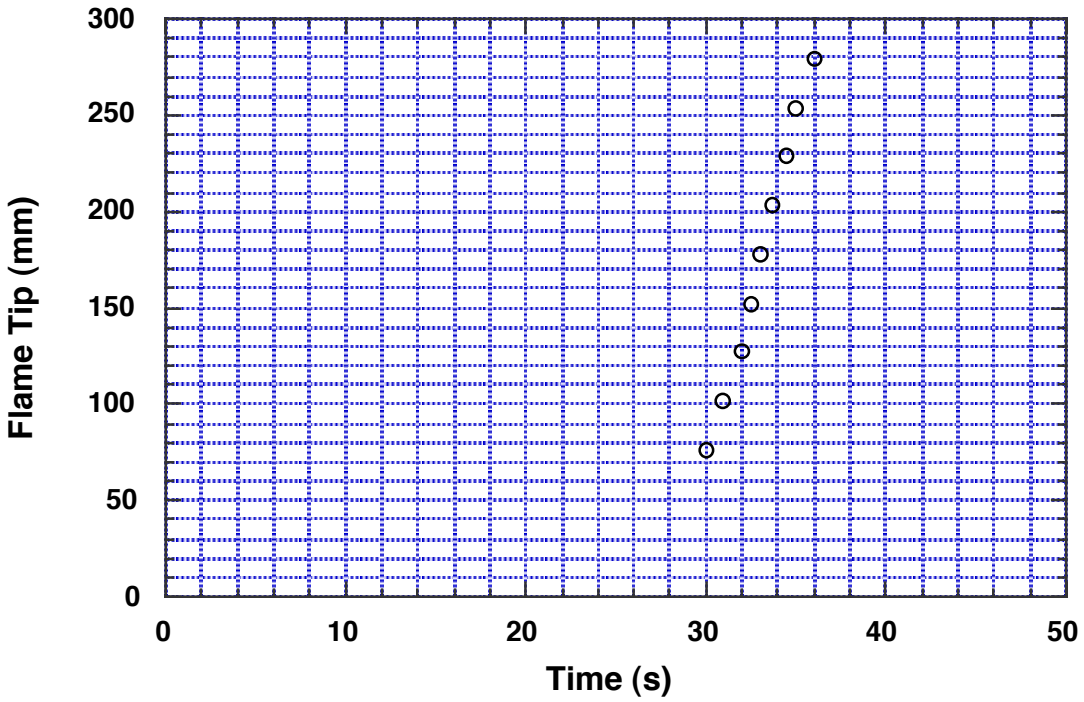

FIGURE 3g. UPWARD FLAME SPREAD, FACING DOWN, ϕ = -60°, NAPKIN

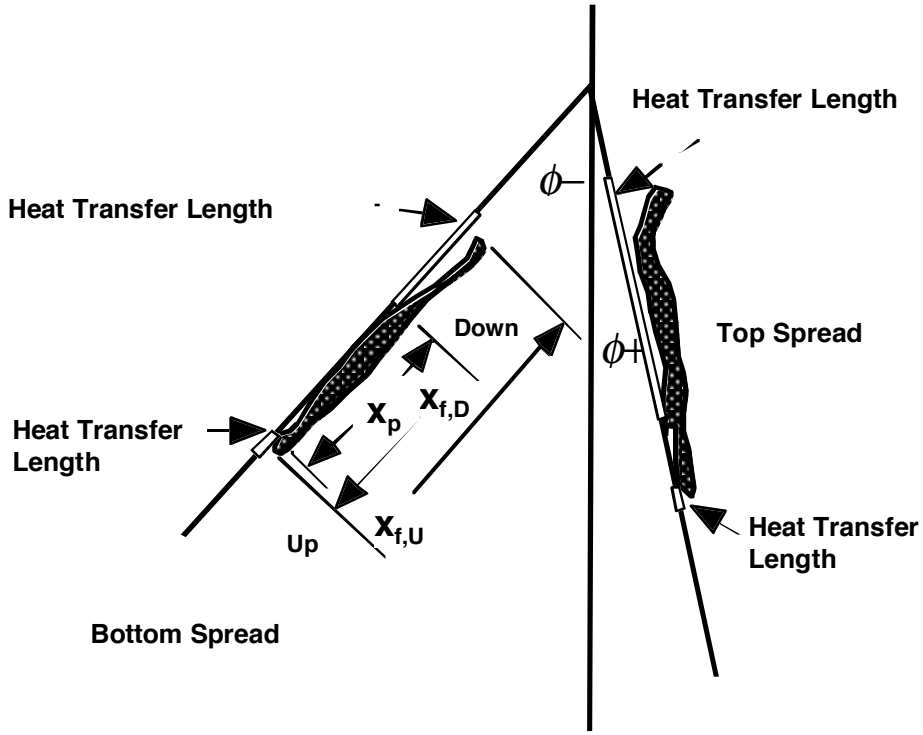

FIGURE 4. SPREAD CONFIGURATIONS AND THEORETICAL NOTATION

Equation 1 follows from an assumption of steady spread rate with a perfectly insulated back face. By considering an average heat flux over the heat transfer length x_f - x_p, equation 1 can be written as

$$v_p = \frac{dx_p}{dt} = \frac{x_f - x_p}{t_{ig}} \tag{2a}$$

where the ignition time is

$$t_{ig} = \frac{\rho \delta c (T_{ig} - T_\infty)}{\dot{q}''}. \tag{2b}$$

A similar result applies to thermally thick solids where the expression for t_{ig} is changed to fit the thick condition.

If we regard x as measured from the point of ignition and include the burnout position x_b (see figure 5), then

$$x_b(t + t_b) = x_p(t) \approx x_b(t) + t_b \frac{dx_b}{dt} \tag{3a}$$

or

$$\frac{dx_b}{dt} = \frac{x_p(t) - x_b(t)}{t_b} \tag{3b}$$

where the burnout time is

$$t_b = \frac{\rho \delta (1 - \mu)}{\overline{\dot{m}''}} \tag{3c}$$

with $\overline{\dot{m}''}$, the average mass loss flux of the volatile fuel and μ, the char fraction.

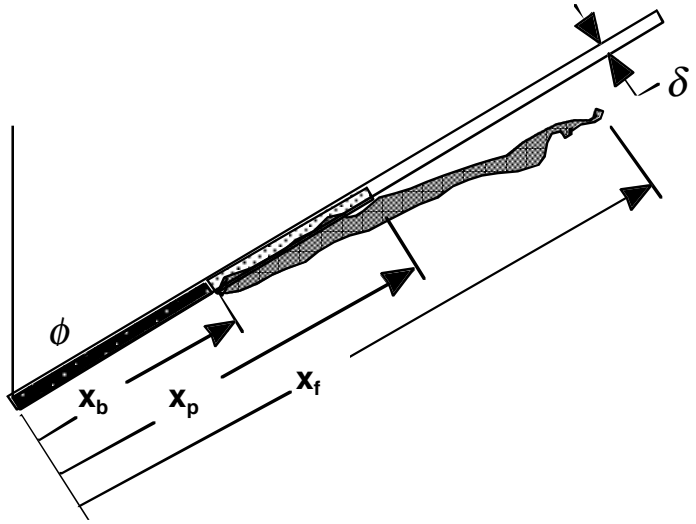

FIGURE 5. UPWARD SPREAD WITH BURNOUT

The complete problem of spread with burnout can be solved by computing the solution to the two ordinary differential equations 2a and 3b. In order to do this the following are needed:

1. material properties: $\rho\delta$, c, T_{ig} , μ,
2. a burn rate relationship for $\dot{m}''$, and
3. a heat flux relationship for $\dot{q}''$.

As an alternative to solving the differential equations, an analysis was performed based on the measured flame length for upward or gravity-assisted flame spread. Figures 6a and 6b give the observed flame lengths for angles of 0°, +30°, +60°, and +90° during spread for the napkin and PET, respectively. The increments shown are 1 inch and the flame shape is drawn to scale. For these experiments, the napkin displayed a uniform flame front as shown in figure 7a, indicative of one-dimensional surface spread. In contrast, the PET flame spread was two-dimensional and was affected by curling in the direction of spread as shown in figure 7b. Since the theoretical results apply to a one-dimensional spread, only the napkin data will be analyzed.

For the gravity assisted analysis, the work of Faeth and coworkers [4, 5, 6] will be used. For the gravity opposed case, the work of Kashiwagi et al. [7, 8] will be used. These works will give the ability to compute the flame heat flux and heat transfer region (x_f - x_p) needed to determine v_p from equation 2. Then a comparison can be made with measured flame speeds.

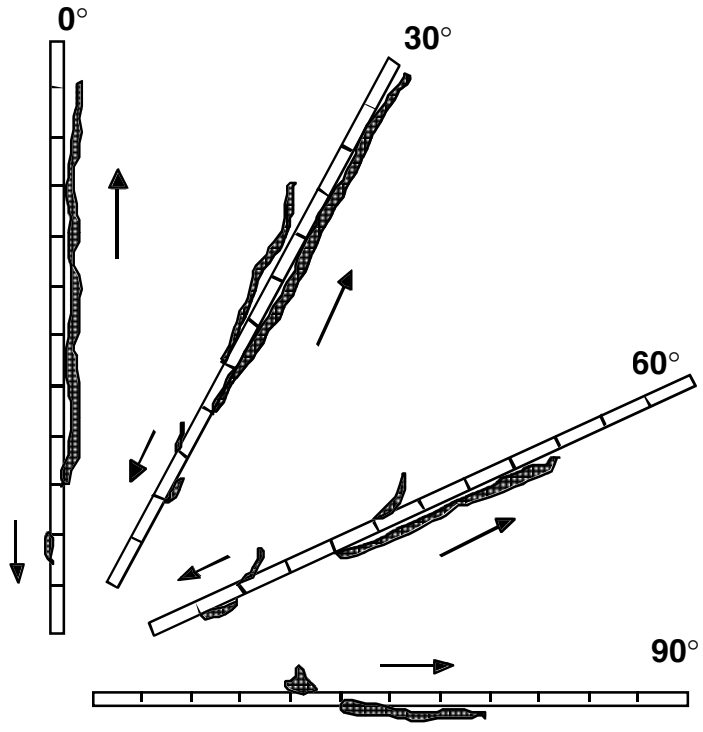

FIGURE 6a. OBSERVED FLAME LENGTHS ON NAPKINS, INCREMENTS 2.5 cm

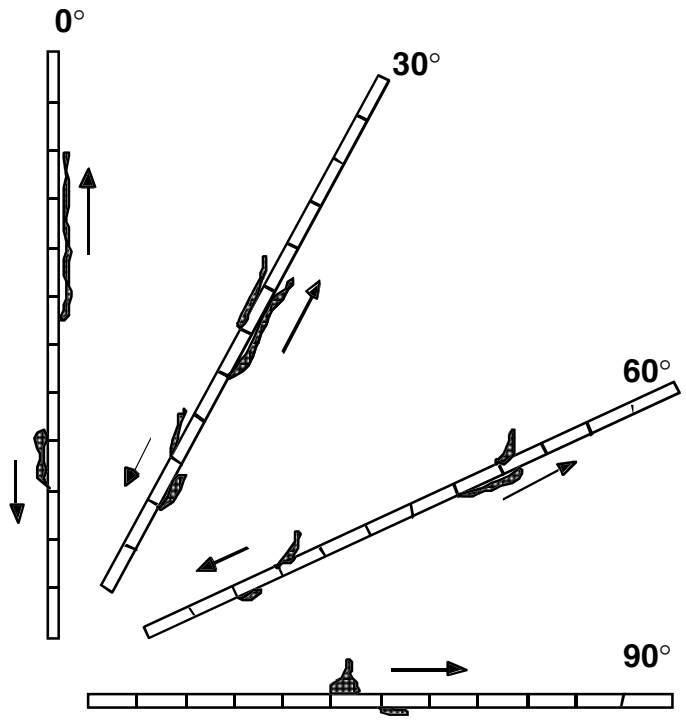

FIGURE 6b. OBSERVED FLAME LENGTHS ON PET FILM, INCREMENTS 2.5 cm

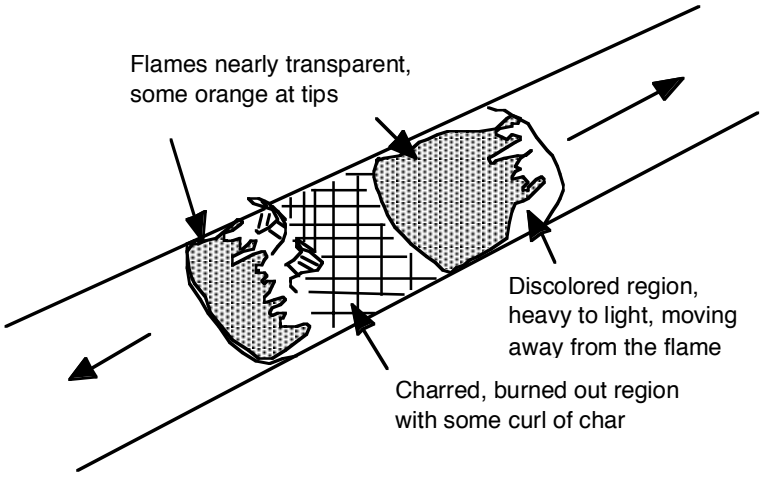

FIGURE 7a. FLAME SPREAD BEHAVIOR ON NAPKINS

GRAVITY ASSISTED FLAME SPREAD. Gravity assisted spread is defined to occur when the component of gravity parallel to the surface is opposite to the spread direction, and consequently the corresponding buoyant force is assisting flame spread. The thesis by Ahmad, under Faeth, will be the chief source of information in making calculations for the gravity assisted burning rate and flame length [5]. In these calculations, the pyrolysis and flame length, x_p and x_f, will be measured from the start of pyrolysis region as shown in figure 4. (These results will be used in the context of figure 5 where x_p is x_f - x_b of figure 5).

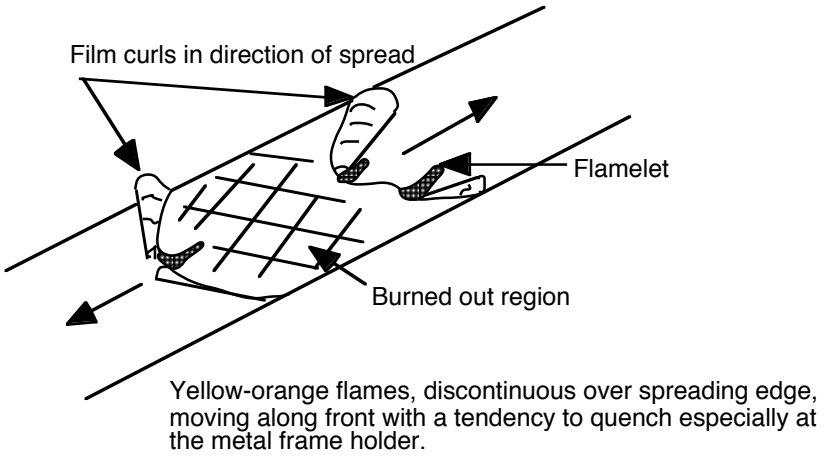

FIGURE 7b. FLAME SPREAD BEHAVIOR ON PET FILM

Reference 5 contains both theoretical and experimental results for both laminar and turbulent flows. The Grashof number, Gr_x, indicating the ratio of buoyant to viscous forces is defined as

$$Gr_x = \frac{g \cos\phi \, x^3}{\nu_\infty^{\,2}} \tag{4}$$

where g is the gravity force per unit mass
x is distance along the surface
ν_∞ is the kinematic viscosity of the combustion products (approximated as air at T_∞).

The onset of turbulence occurs at Gr_x = 0.5 x 10^8 for ϕ = 0 from which equation 4 gives x = 106 mm. Ahmad, however, achieved turbulent flow for x = 51 mm by tripping the boundary layer. The total length of material tested in figure 2 was 300 mm (12 in.). Hence, it is most likely that turbulent conditions prevailed. Nevertheless, laminar analysis will be included especially since it will be shown that laminar flame spread can be much faster than the turbulent case.

The burning rate analysis [4-6] has been based on steady conditions for an evaporating liquid fuel model. Liquid fuels (methanol, ethanol, and propanol) were saturated in an inert porous solid plate to obtain data. The dimensionless coefficients presented herein will always be based on the "best-fit" experimental values for these fuels. The theoretical results will be used to estimate the behavior for other fuel properties. The equations hold as long as boundary layer flows prevail, but as $\phi \rightarrow 90°$ for a plate facing upwards, detachment will occur. Theoretically the solution is said to hold up to ±85° [5].

Definitions. The following parameters used in the analysis are defined here for clarity.

Stoichiometric oxygen to fuel mass ratio, s

Available to stoichiometric oxygen-fuel ratio, $r = \frac{Y_{o,\infty}}{Y_{F,T}} s^{-1}$

$Y_{o,\infty}$ is the free stream oxygen mass fraction

$Y_{F,T}$ is the transferred (solid or liquid) fuel mass fraction

Spalding B Number, $B = \frac{Y_{o,\infty}(\Delta H_c / s)}{L} - \tau_o = \frac{\text{combustion energy}}{\text{evaporation energy}}$

$$\tau_o = \frac{c_g(T_v - T_\infty)}{L}$$

c_g is the heat capacity of the gas

T_v is the wall vaporization temperature

L is the heat of gasification (sensible plus phase change)

$\theta_{FO\,f} = \frac{r(B+1)}{B(r+1)}$ is a flame locus parameter

Prandtl Number, $\Pr = \frac{\nu}{\alpha}$, is the ratio of viscous diffusion to thermal diffusion (taken as 0.73)

Modified Grashof Number, $G_r^* = \left(\frac{L}{4c_p T_\infty}\right) Gr_x$

Laminar. The burning rate per unit area, $\dot{m}''$, can be determined from

$$\frac{\dot{m}'' x \Pr Gr_x^{*-1/4}}{B\mu_\infty} = C_{m,L}(B, \Pr, \tau_o, \theta_{FO_f}) \tag{5}$$

where μ_∞ is the viscosity of the gas (20×10^{-6} N-s) and $C_{m,L}$ is primarily a function of B. Table 2 shows the selected coefficients for the fuels [4-6] with their properties where $C_{f,L}$, $C_{q,L}$, and $C_{q,T}$ are the empirical coefficient for laminar burning rate, laminar heat flux, and turbulent heat flux, respectively. Figure 8 shows an empirical fit as a function of B. The average burning rate over length x can be determined from equation 5 as

$$\overline{\dot{m}''}(x) = \frac{1}{x}\int_0^x \dot{m}'' dx = \frac{4}{3}\dot{m}''(x) \tag{6}$$

TABLE 2. LIQUID FUEL PROPERTIES

Fuel	s	r (air)	L (kJ/g)	τ_o	T_v (K)	ΔH_c (kJ/g)	B	$C_{m,L}$	$C_{f,L}$	$C_{q,L}$	$C_{q,T}$
Methanol	1.51	0.154	1.23	0.044	337	19.1	2.60	0.29	4.8	0.53	0.030
Ethanol	2.10	0.111	0.880	0.087	352	25.6	3.41	0.27	9.0	0.55	0.038
Propanol	2.68	0.087	0.788	0.134	370	29.0	3.71	0.25	11.0	0.59	0.040

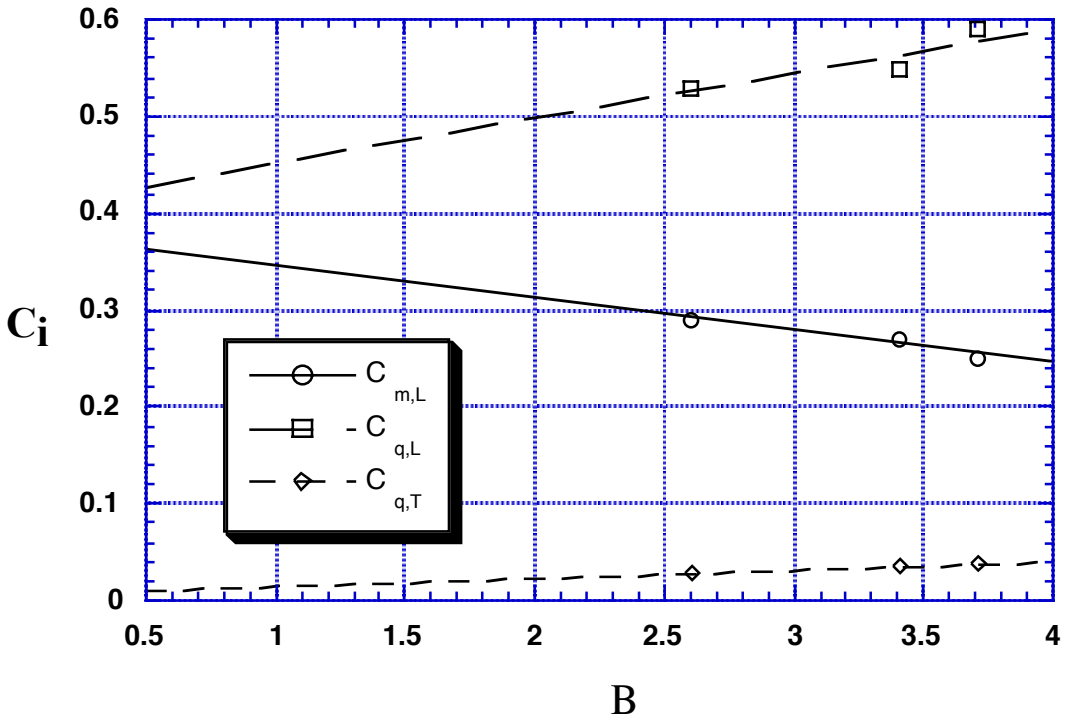

FIGURE 8. EMPIRICAL COEFFICIENTS AS A FUNCTION OF B

The flame length measured from the start of the pyrolysis region is found as

$$\frac{x_f}{x_p} = C_{f,L} \tag{7}$$

where $C_{f,L}$ (table 1) depends on the fuel.

Roper et al. [9] find for a buoyancy controlled slot burner in air at volumetric fuel flow rate per unit length, $\dot{V}_F'$:

$$x_f = 2x10^3 \left[\frac{\beta \dot{V}_F' (T_\infty / T_F)}{\left[0.6 g \left(\frac{T_f}{T_\infty} - 1 \right) \right]^{1/4}} \right]^{4/3} \quad \text{in S.I. units} \tag{8}$$

where T_F and T_f are fuel and flame temperatures, respectively, and β is a function of S, the molar stoichiometric oxidizer to fuel ratio.

for a slot burner:
$$\beta = \frac{1}{4\,inv\left[erf\left(\frac{1}{1+S}\right)\right]} \tag{9a}$$

and for a circular burner:
$$\beta = \frac{1}{\ln\left(1+\frac{1}{S}\right)} \approx S \text{ for large } S. \tag{9b}$$

Rearrangement of equations 7 and 8 show their similarity and allows for some generalizations. From equations 5 and 6 with the energy release rate per unit lateral dimension of the wall

$$\dot{Q}' = \Delta H_c \overline{\dot{m}''} x_p, \tag{10}$$

it can be shown that equation 7 can be written as

$$x_f = \left(\frac{3^{4/3}}{4}\right) C_{f,L} \left[\frac{\mathrm{Pr}}{C_{m,L} B} \frac{c_p T_\infty}{\Delta H_c}\right]^{4/3} \left(\frac{c_p T_\infty}{L}\right)^{1/3} \frac{\ell_c^{\,2}}{\ell_v} \tag{11}$$

The characteristic length scales are the plume convective length,

$$\ell_c = \left(\frac{\dot{Q}'}{\rho_\infty c_p T_\infty \sqrt{g \cos\phi}}\right)^{2/3}, \tag{12}$$

and plume viscous length,
$$\ell_v = \left(\frac{\nu_\infty}{\sqrt{g \cos\phi}}\right)^{2/3}. \tag{13}$$

By recognizing
$$BL \approx Y_{o,\infty} \Delta H_{ox}$$
$$\Delta H_{ox} = \Delta H_c / s \approx 13.6 kJ/g,$$

equation 11 can be approximated as

$$x_f \approx \frac{(3\,\mathrm{Pr})^{4/3}}{4 Y_{o,\infty}^{\,1/3}} \left(\frac{c_p T_\infty}{\Delta H_{ox}}\right)^{5/3} \left(\frac{C_{f,L}}{B C_{m,L}^{\,4/3} s}\right) s^{7/3} \frac{\ell_c^{\,2}}{\ell_v} \tag{14}$$

It is found that $\frac{C_{f,L}}{B C_{m,L}^{\,4/3} s} \approx 7.0 \pm 0.5$ for the three experimental liquid fuels. Substituting $T_\infty = 298$ K, $c_p = 10^{-3}$ kJ/g, and Pr = 0.73, the Ahmad-Faeth equation can be expressed as

$$x_f = 0.023 \frac{s^{7/3}}{Y_{o,\infty}^{\,1/3}} \frac{\ell_c^{\,2}}{\ell_v}. \tag{15}$$

The result by Roper et al., equation 8, can also be put into this form (dropping the T_f-term)

$$x_f = C_R\left[\beta \cdot s \cdot \left(\frac{T_\infty}{T_F}\right) \cdot \left(\frac{c_p T_\infty}{\Delta H_{ox}}\right)\right]^{4/3} \frac{\ell_c^{\,2}}{\ell_v}$$

where C_R is a constant.

If the approximation in equation 9b is used, Roper's equation becomes

$$x_f \approx C_R\left[\left(\frac{T_\infty}{T_F}\right)\left(\frac{c_p T_\infty}{\Delta H_{ox}}\right) S^2\right]^{4/3} \frac{\ell_c^{\,2}}{\ell_v} \tag{16}$$

which is very similar to equation 14.

The heat flux in the pyrolysis region is approximately constant and determined by

$$\dot{q}''_{p,L} = \overline{\dot{m}''}(x_p) \cdot L \tag{17}$$

In the "over-fire" region or where the flame extends $(x_f - x_p)$, the heat flux can be approximated as constant by

$$\frac{\dot{q}''_{f,L} x_p Pr Gr_{x_p}^{\,-1/4}}{B, L \mu_\omega} = C_{q,L} \tag{18}$$

where $C_{q,L}$ is given in table 1 and figure 8. A typical result from Ahmad [5] is shown in figure 9 and illustrates the complete distribution within and beyond the flame.

<u>Turbulent</u>. The corresponding turbulent results derived from reference 5 follow.

Burning Rate:

$$\frac{\overline{\dot{m}''} x \,\mathrm{Pr}^{0.27}\, Gr_x^{*-0.4}}{\mu_\infty} = \frac{0.0285}{\Sigma} \tag{19a}$$

where

$$\Sigma = \left[\frac{1+B}{B \cdot \ln(1+B)}\right]^{1/2} \left[\frac{1 + 0.5\,\mathrm{Pr}/(1+B)}{3(B+\tau_o)\eta_f + \tau_o}\right]^{1/4} \tag{19b}$$

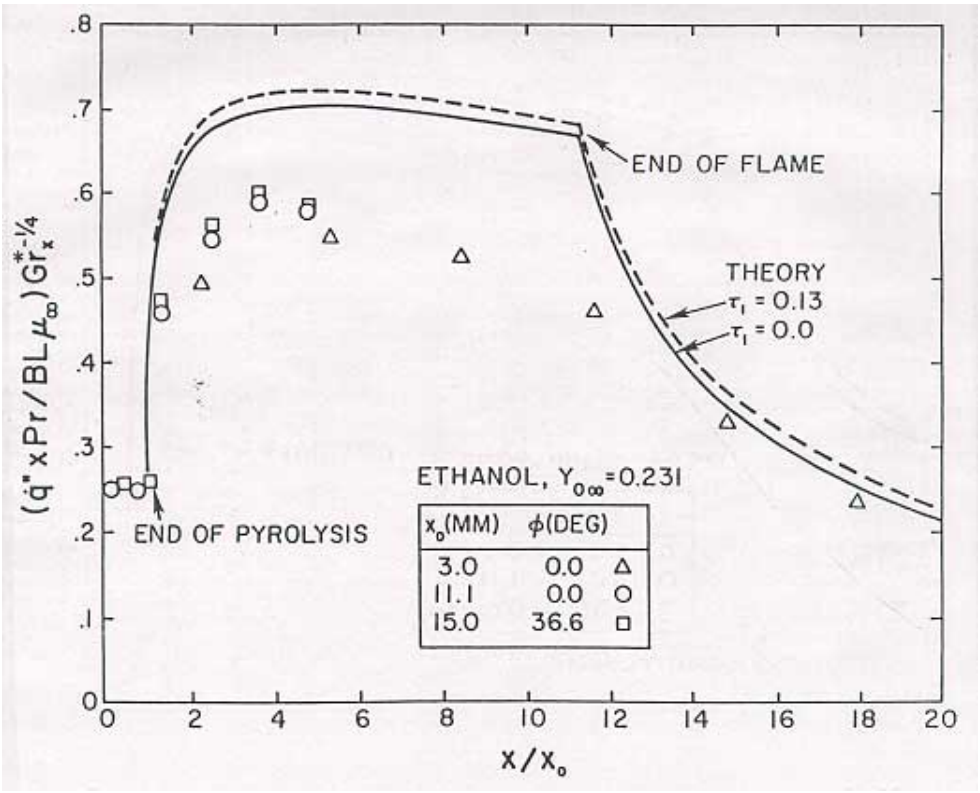

FIGURE 9. WALL HEAT FLUX

$$\eta_f = 1 - \theta_{F0_f}^{1/3} \tag{19c}$$

with $\eta_f \approx 0.43$ for methanol and $\eta_f \approx 0.33$ for cellulose and PET.

Flame Height:

$$x_{f,T} = \frac{1.02\ell_c}{Y_{o,\infty}(1 - X_r)^{1/3}} \tag{20}$$

where X_r is the flame radiative fraction. Values for the flame radiative fraction for the liquid fuels were calculated from the total energy release rate and the radiative heat flux lost to the wall and the surroundings as tabulated in table 7 of reference 5. These were found to range from 0.06 to 0.12 with an average of about 0.10 for all of the liquids.

Figure 10 shows this result for flame height plotted against data taken from reference 5. The flame length was inferred from distributions of the wall heat flux at the position where the measured heat flux significantly dropped in the over-fire region. Equation 20 is consistent with well known results for wall flames in air (e.g., Fernandez-Pello [10] where the coefficient of ℓ_c ranges from 4.5 to 8.0). The dependencies in $Y_{o,\infty}$ and X_r come from results for line fires by Quintiere and Grove [11]. Using values $Y_{o,\infty} = 0.233$ and $X_r = 0.1$, the coefficient is computed

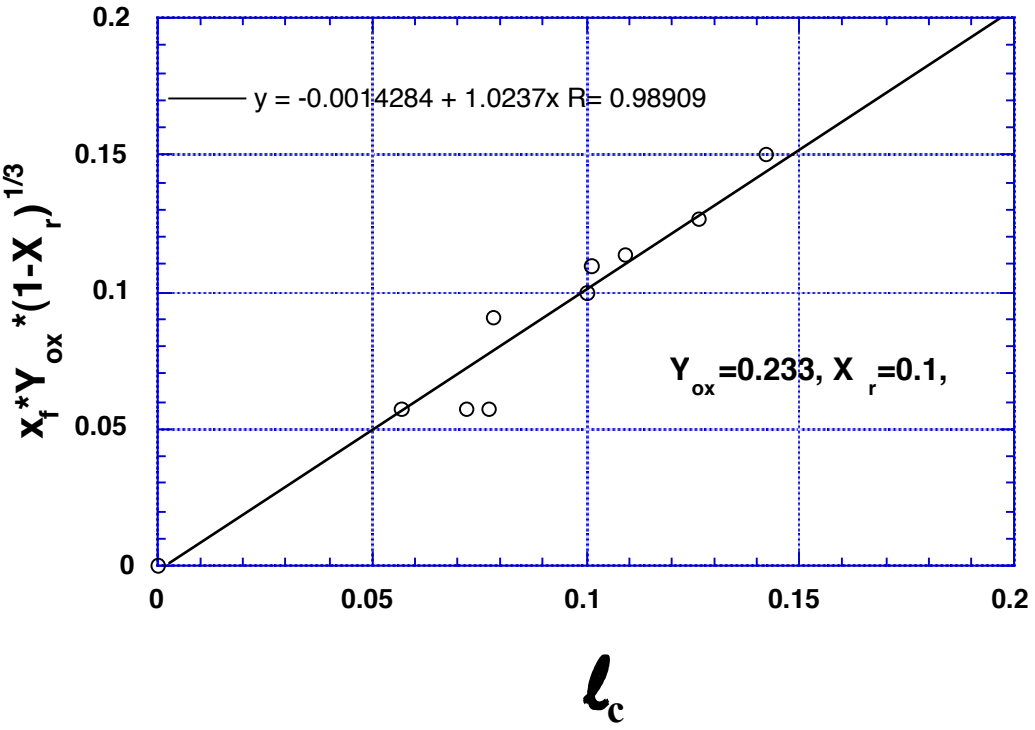

FIGURE 10. WALL FLAME HEIGHT CORRELATION BASED ON DATA FROM AHMAD [5]

as 4.5 in equation 20. Since the interpretation of the Faeth et al. [4-6], flame length data is based on the position of a sharp decrease in the heat flux; this coefficient of 4.5 likely corresponds to a length within the flickering flame zone.

Flame Heat Flux:

The heat flux in the over-fire region is based on the total incident heat flux. An empirical result for the average flame heat flux is given by

$$\frac{\overline{\dot{q}''_{f,T}} x_p \Pr Gr_x^{*-0.4}}{BL\mu_\infty} = C_{q,L} \tag{21}$$

with the empirical correlation for the coefficient given in figure 8. Results from Ahmad [5] are shown in figure 11 for ethanol. They show the complete heat flux distribution into the wall plume beyond the flame. Both the turbulent and laminar correlations for flame heat flux assume constant heat flux over the flame region and ignore the contribution by the wall plume.

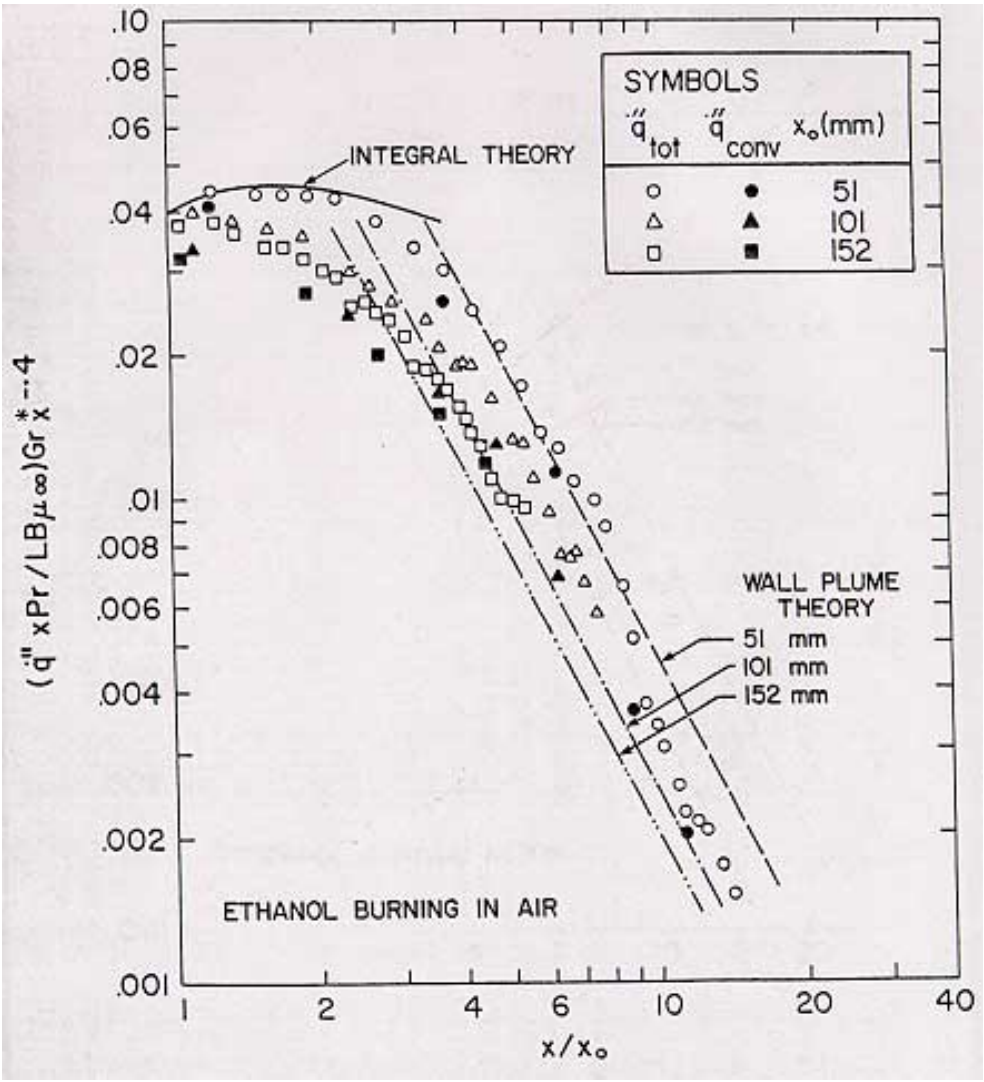

FIGURE 11. WALL HEAT FLUX FOR ETHANOL TAKEN FROM AHMAD [5]
(X_O is pyrolysis length)

GRAVITY OPPOSED FLAME SPREAD. For opposed flow flame spread, the flame heat transfer is needed at the "nose" of the flame as depicted in figure 4. In the theoretical solution by DeRis [12] for thermally thin (i.e., ≤ 1- to 2-mm) materials, the opposed flow flame speed is

$$v_p = \frac{\sqrt{2}k_g\left(T_f - T_{ig}\right)}{(\rho\delta)c\left(T_{ig} - T_\infty\right)} \tag{22}$$

where k_g is the thermal conductivity of the gas.

No dependence on gravity induced flow velocity occurs. The flame temperature can be regarded as nearly constant provided there are gas phase retardants or diluents that can decompose from the material. The polymethyl-methacrylate (PMMA) data of Ito and Kashiwagi [8] should have

this character enabling their data on heat flux and the flame heating region to be somewhat generic, or an upper limit in the least for heat flux. Their results for the forward heat flux distributions are shown in figure 12 as a function of angle θ, the complement of ϕ $(\phi = -90 - \theta)$. The heat flux measured is the absorbed or net surface heat flux. An average heat flux was determined by the area under the curves for $\dot{q}'' \geq 20 kW/m^2$ and the heat transfer region $(x_f - x_p)$ defined by length corresponding to $20\,\mathrm{kW/m^2}$. These results are plotted in figure 13 for downward as well as upward spread for the range of their data. Since the vaporization temperature reported for this PMMA was 380°C, corresponding to a re-radiation flux of 10 kW/m^2, the incident flux could be up to 10 kW/m^2 higher. The lower limit values as shown in figure 13 will be used in the analysis to follow.

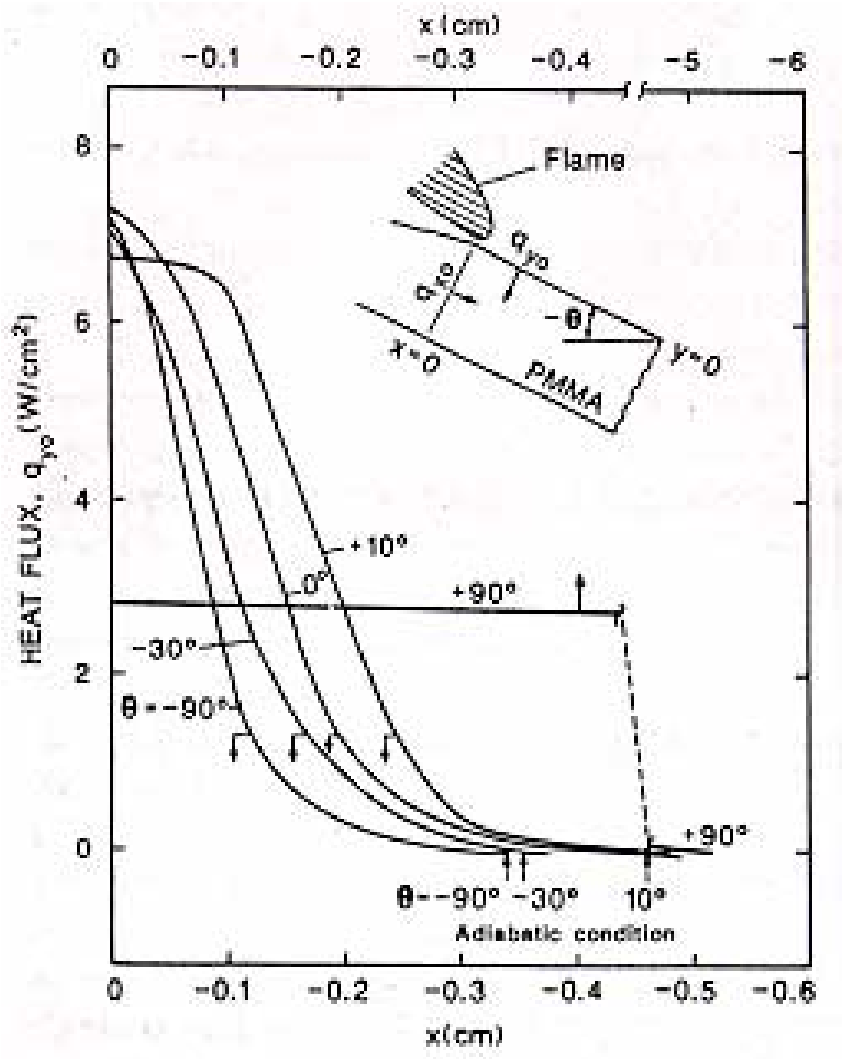

FIGURE 12. HEAT FLUX AHEAD OF THE FLAME FROM ITO AND KASHIWAGI [8]

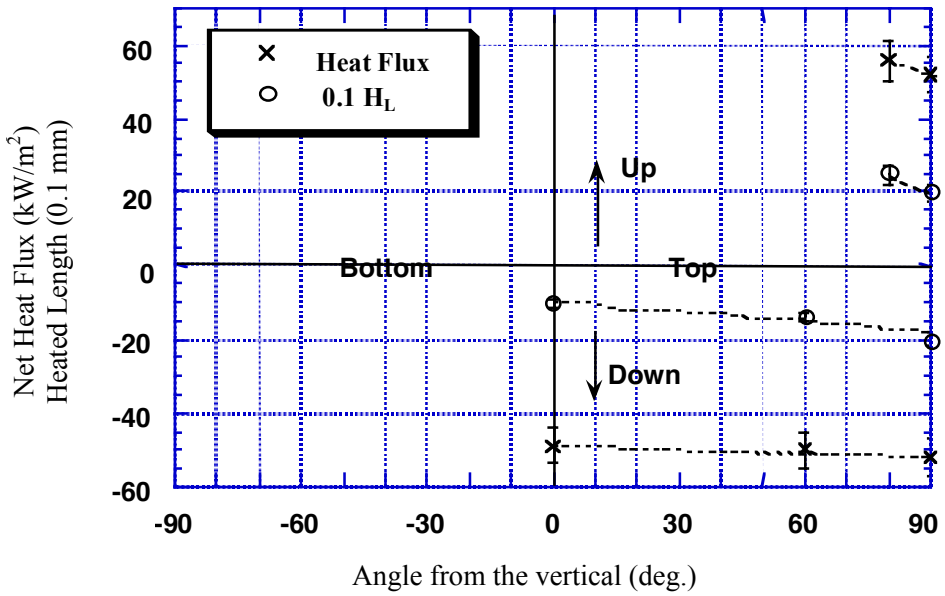

FIGURE 13. AVERAGE FLAME HEAT FLUX AND HEATED LENGTH IN OPPOSED FLOW FLAME SPREAD DERIVED FROM ITO AND KASHIWAGI [8]

RESULTS

The computations for flame spread will be made using the equations and data presented in the previous section. Properties will be assembled, as best estimates, for the brown paper towel (napkin) and the insulation film (MPET).

EXPERIMENTAL. The experimental results are shown in figures 14 and 15 for the napkin and MPET. The frequency of extinguishment of the flame front during propagation over the 30.5-cm sample lengths (figure 14) shows the wide variation of the MPET in its ability to maintain sustained flame spread. It appears the highest frequency of extinguish occurred for spread on the top or upward facing surface of the MPET. In contrast, the napkin was nearly free of extinguishment. Despite the frequent extinguishment of the MPET, the measured flame speeds for the MPET and napkin are very similar. Downward spread on the top surface is nearly constant from 0° to +90° at about 1-2 mm/s. Downward spread on the bottom surface distinctly increases at about -60°. This transition is consistent with results by Kashiwagi and Newman [7] for 1-mm α-cellulose sheets. The upward burning on the top surface shows an increase in speed as the sample becomes more vertical with a transition between 30° and 60°. Kashiwagi and Newman [7] report that the flame on the top surface separates from the surface at $\phi = 60°$ and remained more boundary layer-like below 60°. Figures 6a and 6b reveal this as well. The upward spread in the bottom surface is most severe since it maintains its boundary layer character for all angles up to -90° and results in long flame lengths. Although most of the data remained steady, upward spread near the vertical was accelerating with speeds of 30 – 60 mm/s.

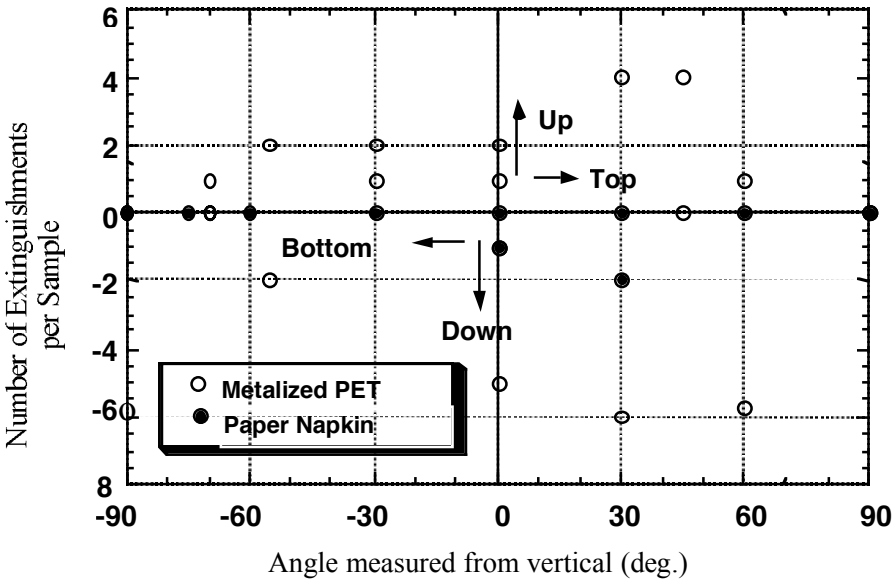

FIGURE 14. FREQUENCY OF EXTINGUISHMENT DURING FLAME SPREAD

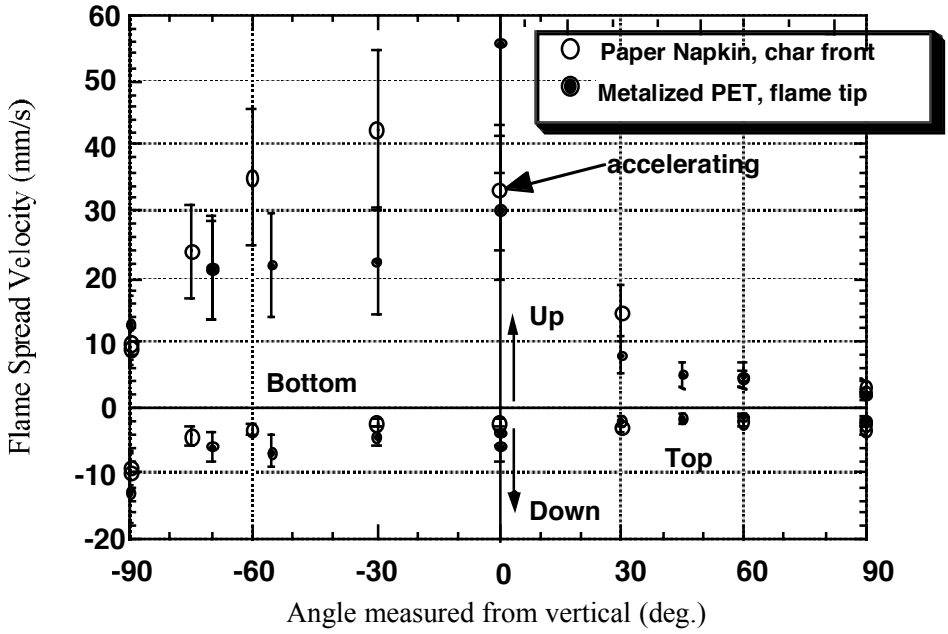

FIGURE 15. FLAME SPREAD VELOCITY

THEORETICAL. The flame speeds were computed as a function of angle, orientation, and direction. While they could be computed from equations 2 and 3 together with the flame length and heat flux correlations, it was decided to use measured flame lengths (for upward spread) to compute v_p directly from equation 2. For turbulent upward spread, the procedure was to compute $\overline{\dot{m}''}_p$ from equation 20, x_p from equation 19, and $\dot{q}''_f$ from equation 18. The corresponding laminar speeds, for the measured flame length, will not be reported. They were significantly higher than the turbulent speeds. Downward and nearly horizontal spread on the

top surface was computed from the heat flux and flame-heated length as given in figure 13. The ignition time was computed from equation 2b.

Properties needed in the computations were estimated from literature values and are given in table 3. The effect of temperatures on specific heat was estimated by $c = 1.5c_\infty$.

TABLE 3. THIN-MATERIAL PROPERTIES

Material	$\rho\delta$ (kg/m^2)	c_∞ (kJ/kg-K)	L (kJ/kg)	$\Delta H_{c,\,actual}$ (kJ/g)	T_{ig} °C	B –	X_r –
Napkin	0.0374	1.34[1]	3000[3]	11,400[4]	350[6]	0.91	0.1
MPET	0.0320	1.0[2]	3000[3]	21,300[2]	450[5]	0.86	0.1

[1] Incoperra and DeWitt [13]
[2] Babrauskas [14]
[3] Lyon [15]
[4] Tewarson [16]
[5] Van Krevelin [17]
[6] Kashiwagi and Newman [7]

Figure 16 gives the flame length as measured parallel to the surface and in the direction of spread from the start of pyrolysis. These lengths were estimated from video frames and are not unique when upward acceleration occurred. These values were used to compute the gravity assisted flame speeds. The flame lengths given in figure 16 are the total flame length including the pyrolysis region and should not be confused with the flame extension or heat transfer length, x_f-x_p.

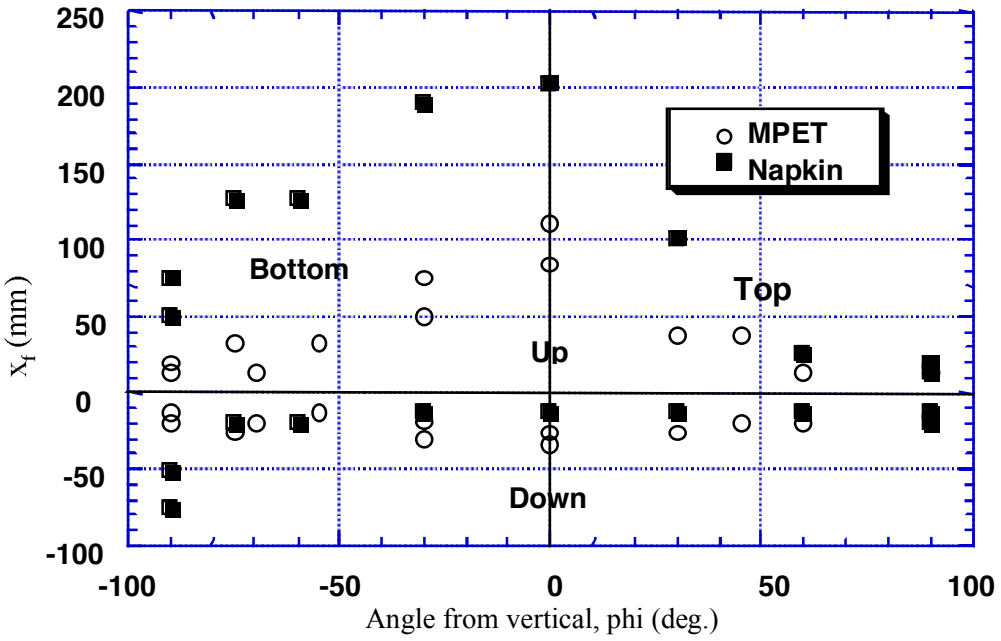

FIGURE 16. FLAME LENGTH MEASURED PARALLEL TO THE SURFACE

Gas phase properties were taken as:

ρ_∞ = 1.2 kg/m^3
$c_{p,\infty}$ = 1.0 kJ/kg-K (air stream)
T_∞ = 298 K
ν_∞ = 15.3 × 10^{-6} m^2/s
Pr = 0.73
c_g = 1.4 kJ/kg-K (fuel stream)

It can be shown that in units of kg, kJ, m, and s the equations needed to predict gravity assisted flame spread can be expressed as follows:

$$\left(\overline{\dot{m}''}x_p\right) = 116(\cos\phi)^{1/2} x_{f,T}^{3/2} / \Delta H_c \ ,$$

$$x_p = 454.3\left(\left(\overline{\dot{m}''}x_p\right)\Sigma\right)^{5/6} / (L\cdot\cos\phi)^{1/3},$$

$$\overline{\dot{m}''} = \left(\overline{\dot{m}''}x_p\right) / x_p ,$$

$$\overline{\dot{q}_p''} = \overline{\dot{m}''}L \text{, and}$$

$$\dot{q}_f'' = C_{q,L} BL(\cos\phi\cdot L)^{2/5} x_p^{1/5}.$$

Then we have sufficient information to compute the speed from equation 2, $v_p = \dfrac{x_f - x_p}{t_{ig}}$. For gravity opposed spread, equation 2 can be directly implemented from the flame heat transfer information given in figure 13. The computed results are shown in figure 17 and labeled according to the correlations of Ahmad and Faeth (AF) and Ito and Kashiwagi (IK). The predictive results appear to follow the data with reasonable agreement.

DISCUSSION

From figure 17, it is obvious from both theory and experiment that the most serious flame spread hazard, in terms of speed, is vertical upward spread. Flame spread downward, on either top or bottom, is less than 4 mm/s for all angles except for the bottom horizontal orientation at which it nearly doubles to 9 mm/s. Upward spread on the bottom is generally faster than upward spread on the top.

The flame heat flux is higher (~50 kW/m^2) for downward or gravity opposed spread than for upward or gravity assisted spread with heat fluxes of ~10-20 kW/m^2 for angles of 0° to ±60°.

The relatively large flame heated length for upward spread, roughly 4 cm, causes the higher spread rate for this orientation. Between -75° and 30°, Gr_{xp}^* was at least 10^7 implying turbulent flow for all of the gravity-assisted cases.

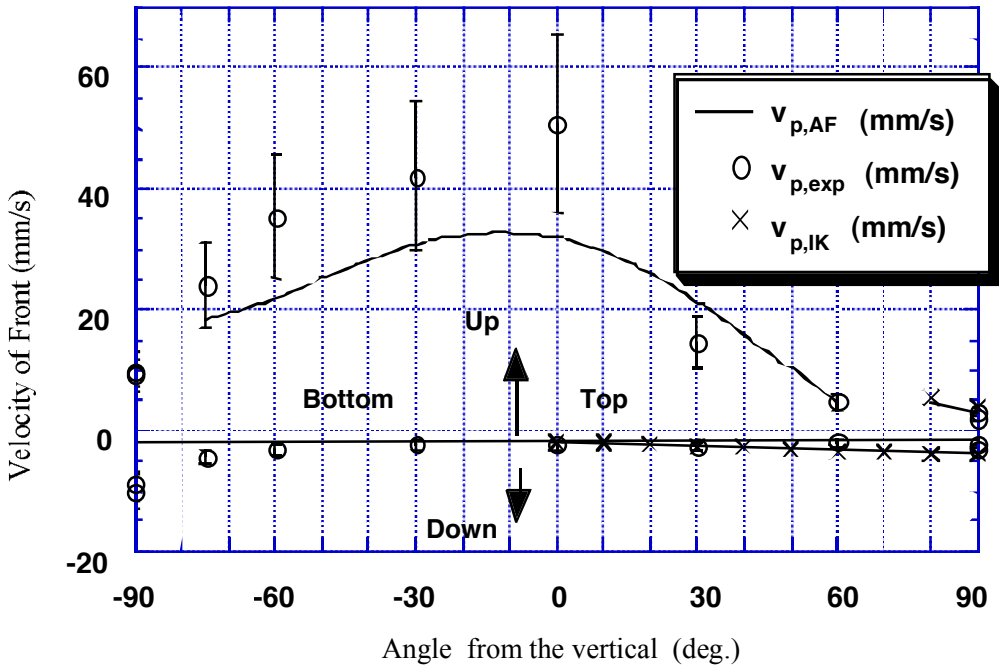

FIGURE 17. COMPARISON OF PREDICTED AND MEASURED FLAME SPEEDS FOR THE NAPKIN

Computed results for the MPET film gave similar results to the napkin material. However, the one-dimensional flame spread theory would not apply to the two-dimensional burning as illustrated in figure 7b.

Although laminar burning conditions did not appear relevant, computations showed that the gravity assisted cases yielded heat fluxes as high as 50 kW/m^2 and speeds up to 500 mm/s. This suggests that in small flame tests, such as Bunsen burner ignition tests, the initial flame speed could be high due to laminar conditions. This will occur before the onset of turbulent flow. Such results can be misleading and erratic since many sources of disturbance can influence the transition to turbulent flames.

Finally, it should be emphasized that the flame spread speeds reported here apply to comparable conditions of scale and ambient environment. Where accelerating flames might occur for larger scale upward conditions, higher velocities will prevail. Where thermal environments in a developing compartment fire might occur, thermally enhanced speeds will occur.

CONCLUSIONS

This study has shown the effect of orientation on flame spread over thin films. It has shown that satisfactory predictive results could be achieved based on general correlations and data in the literature. In the process of executing this analysis, relationships for flame length were developed for both laminar and turbulent burning of walls. These are consistent with other results in the literature.

REFERENCES

1. Cahill, P., "Evaluation of Fire Test Methods for Aircraft Thermal Acoustical Insulation," DOT/FAA/AR-97/58, September 1997.

2. Cahill, P., Private Communication, FAA, Atlantic City International Airport, NJ, 1999.

3. Markstein, G. H. and DeRis, J., "Upward Fire Spread Over Textiles," 14th Symp. (Int.) on Combustion, The Combustion Institute, p. 1085, 1973.

4. Ahmad, T., Groff, E. G., and Faeth, G. M., "Fire-Induced Plumes Along a Vertical Wall: Part II: The Laminar Combusting Region," Mech. Engrg. Dept., The Pennsylvania State Univ., July 1977.

5. Ahmad, T., "Investigation of the Combusting Region of Fire-Induced Plumes Along Upright Surfaces," Ph.D. Thesis, The Pennsylvania State Univ., August 1978.

6. Ahmad, T. and Faeth, G. M., "Turbulent Wall Fires," 17th Symposium (Int.) on Combustion, The Combustion Institute, p. 1149, 1978.

7. Kashiwagi, T. and Newman, D. L.," Flame Spread Over an Inclined Thin Fuel Surface," *Combustion and Flame*, **26**, p. 163, 1976.

8. Ito, A. and Kashiwagi, T., "Characterization of Flame Spread Over PMMA Using Holographic Interferometry Sample Orientation Effects," *Combustion and Flame*, **71**, p. 189, 1988.

9. Roper, F.G., Smith, C., and Cunningham, A. C., "The Prediction of Laminar Jet Diffusion Flame Sizes: Part II: Experimental Verification," *Combustion and Flame*, **29**, p. 227, 1977.

10. Fernandez, Pello, A. C., " The Solid Phase," in *Fundamentals of Fire and Combustion*, G. Cox, ed., Academic Press, London, 1995.

11. Quintiere, J. G. and Grove, B. S., "A Unified Analysis for Fire Plumes," 27th Symp. (International) on Combustion, The Combustion Institute, p. 2757, 1998.

12. DeRis, J., "The Spread of Laminar Diffusion Flame," 12th Symp. (Int.) on Combustion, The Combustion Institute, p. 241, 1969.

13. Incropera, F.P. and DeWitt, D.P., *Fundamentals of Heat and Mass Transfer*, 3rd ed., John Wiley & Sons, NY, p. A14, 1990.

14. Babrauskas, V., "Related Quantities," in *Heat Release in Fires*, V. Babrauskas and S.J. Greyson, ed., Elsevier Applied Science, London, p. 214, 1992.

15. Lyon, R.E., "Solid-State Thermochemistry of Flaming Combustion," DOT/FAA/AR-99/56, July 1999.

16. Tewarson, A., "Generation of Heat and Chemical Compounds in Fires," in *SFPE Handbook of Fire Protection Engineering,* 2nd ed., NFPA, Quincy, MA, pp. 3-78, 1995.

17. Van Krevelin, D.W., *Properties of Polymers*, Elsevier, Amsterdam, p. 642, 1990.